Room Temperature Electroluminescence from Mechanically Formed van der Waals III–VI Homojunctions and Heterojunctions

*Nilanthy Balakrishnan, Zakhar R. Kudrynskyi, Michael W. Fay, Garry W. Mudd, Simon A. Svatek, Oleg Makarovsky, Zakhar D. Kovalyuk, Laurence Eaves, Peter H. Beton, and Amalia Patanè**

Room temperature electroluminescence from semiconductor junctions is demonstrated. The junctions are fabricated by the exfoliation and direct mechanical adhesion of InSe and GaSe van der Waals layered crystals. Homojunction diodes formed from layers of p- and n-type InSe exhibit electroluminescence at energies close to the bandgap energy of InSe (Eg = 1.26 eV). In contrast, heterojunction diodes formed by combining layers of p-type GaSe and n-type InSe emit photons at lower energies, which is attributed to the generation of spatially indirect excitons and a staggered valence band lineup for the holes at the GaSe/InSe interface. These results demonstrate the technological potential of mechanically formed heterojunctions and homojunctions of direct-bandgap layered GaSe and InSe compounds with an optical response over an extended wavelength range, from the near-infrared to the visible spectrum.

1. Introduction

Over recent years there has been a resurgence of interest in exfoliable layered crystals[1] following their integration into graphene-based devices.[2–6] These materials are often referred to as van der Waals (vdW) solids due to the weak interlayer coupling. Atomically thin layers of large band gap insulators such as hexagonal boron nitride have been exploited as tunnel barriers,[5] substrates for graphene,[6] and as quasi-epitaxial protective layers,[4,5] while metal chalcogenides such MoS_2 and WSe_2 are attracting increasing interest as optoelectronic materials.[3,7–10] It is now established that these dichalcogenides have a thickness-dependent electronic band structure, including a transition from indirect- to direct-band gap for single monolayers, a property that has stimulated recent studies of photoconductivity and photovoltaic effects.[7–10] By exploiting the ease with which atomically thin layers of these materials can be produced by mechanical exfoliation, it is now possible to assemble van der Waals heterostructures layer by layer, with properties that are quite distinct from those of the bulk starting materials. Among the vdW crystals, the III–VI layered semiconductors, such as GaSe and InSe, provide an important class of direct-band gap semiconductors.[11–16] Recent work has included the exfoliation[12] and growth by a vapor phase technique[13] of thin films of GaSe, the demonstration of strong quantum confinement effects in InSe,[14,15] whose direct-band gap can be tuned in the near infrared spectral range when the crystals are exfoliated into nanometer-thick flakes,[14] and the direct-indirect band gap crossover occurring in the single monolayer limit.[16] These properties differ from those of other vdW crystals (e.g., MoS_2, WS_2...), which become direct only as single monolayers.[17,18] Despite their promise as optoelectronic materials, electroluminescence (EL) has to date not been reported in the III–VI layered crystal junctions, and, to our knowledge, has not yet been reported for any vdW heterostructure fabricated using exfoliation and mechanical adhesion between layered crystals.

In this work we demonstrate room temperature electroluminescence from van der Waals semiconductor junctions with atomically flat interfaces, which are fabricated by exfoliation and direct mechanical adhesion of III–VI layered crystals. Homojunction diodes formed from layers of *p*- and *n*-type InSe exhibit EL at energies ($h\nu$ ~ 1.23 eV) close to the band gap energy of InSe (E_g = 1.26 eV). In contrast, heterojunction diodes formed by combining layers of *p*-type GaSe and *n*-type InSe emit photons at lower energies ($h\nu$ = 1.1–1.2 eV), which we attribute to the generation of spatially indirect excitons and a staggered valence band lineup for the holes at the GaSe/InSe interface. Our results demonstrate the technological potential

N. Balakrishnan, G. W. Mudd, S. A. Svatek, O. Makarovsky, L. Eaves, P. H. Beton, A. Patanè
School of Physics and Astronomy
The University of Nottingham
Nottingham NG7 2RD, UK
E-mail: amalia.patane@nottingham.ac.uk

M. W. Fay
Nottingham Nanotechnology and Nanoscience Centre
The University of Nottingham
Nottingham NG7 2RD, UK

Z. R. Kudrynskyi, Z. D. Kovalyuk
Institute for Problems of Materials Science
The National Academy of Sciences of Ukraine Chernivtsi
58001, Ukraine

DOI: 10.1002/adom.201400202

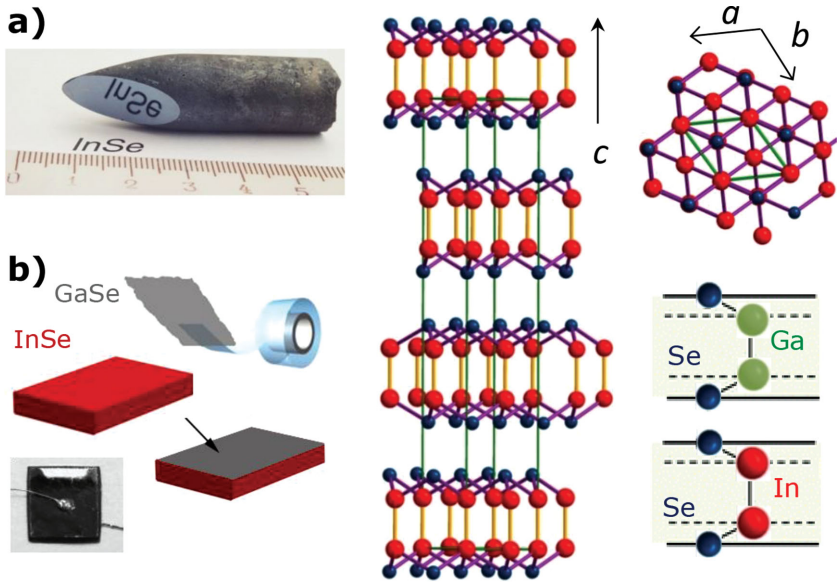

Figure 1. (a) Optical image of a Bridgman-grown InSe ingot and crystal structure of rhombohedral γ-InSe. (b) Exfoliation and mechanical adhesion used to fabricate junctions based on InSe and GaSe, and optical image of a junction device.

of mechanically formed heterojunctions and homojunctions of direct-band gap layered III–VI compounds. These can enable tunable and strong optical response over an extended wavelength range, from the near-infrared (NIR) to the visible (VIS) spectrum; it should also be possible to achieve different band alignments and potential profiles by combining different layered semiconductors, and by selecting the doping, *n*- or *p*-type, of the component layers, which cannot be yet achieved in other van der Waals crystals.

2. Results and Discussion

Our samples are prepared from bulk Bridgman-grown crystals of rhombohedral γ-InSe and hexagonal ε-GaSe polytypes. The primitive unit cells of γ-InSe and ε-GaSe contain three and two layers, respectively, each consisting of four closely packed, covalently bonded, monoatomic sheets in the sequence Se-In-In-Se for InSe (**Figure 1**a) or Se-Ga-Ga-Se for GaSe. Along the *c*-axis, the primitive unit cells of γ-InSe and ε-GaSe have lattice parameters of c_{InSe} = 24.961 Å and c_{GaSe} = 15.949 Å. Within each *a*-*b* plane, atoms form hexagons with lattice parameter a_{InSe} = 4.002 Å and a_{GaSe} = 3.755Å. For the heterojunction, we used *n*-InSe and *p*-GaSe crystals with room temperature concentrations of electrons and holes of 10^{15} cm^{-3} and 10^{13} cm^{-3}, respectively, which were determined from separate Hall effect measurements.[19] For the homojunction, the undoped and intentionally Cd-doped InSe crystals have majority carrier concentrations of 10^{15} cm^{-3} (*n*-type) and 10^{13} cm^{-3} (*p*-type).[20] The cleaved facets of InSe layered crystals are atomically smooth, contain a low-density of surface states and have stable and reproducible photoluminescence properties (see Supporting Information S1).

Flakes with areas between 1 μm^2 to ~ 1 cm^2 and with thicknesses from 1 nm to 10 μm were prepared from as-grown crystals by mechanical exfoliation using adhesive tape. An individual large (~1 cm^2) flake of thickness of ~1–10 μm was then laid onto another layered crystal so that the adhesive van der Waals force between the layers forms an homojunction (e.g., *n*-InSe on *p*-InSe) or an heterojunction (e.g., *p*-GaSe on *n*-InSe). Indium Ohmic contacts were then formed on the top and bottom layers, Figure 1b. As illustrated in **Figure 2**a,b for a *p*-GaSe/*n*-InSe heterojunction, cross-sectional images acquired using transmission electron microscopy (TEM) and high-resolution TEM (HRTEM) show an atomically flat interface between the layers; elemental mapping using energy-dispersive X-ray (EDX) spectroscopy reveals a well-defined, abrupt transition going from the InSe to the GaSe layer along the *c*-axis (Figure 2c); also, the Fourier analysis of the HRTEM images indicate that the layers are generally misaligned in the plane perpendicular to the *c*-axis (see Supporting Information S2). These structural and compositional studies provide evidence for the high-quality of the crystal surfaces and the weak interface interaction between the different layered crystals, which form an abrupt junction despite the simple mechanical contact method used to form the junction and the large lattice mismatch, i.e., $\varepsilon = [a_{InSe} - a_{GaSe}]/a_{InSe} \approx 6\%$, between InSe and GaSe.

The room temperature current–voltage characteristics, *I*–*V*, of the InSe homojunctions fabricated using the van der Waals mechanical contact technique show rectification with low leakage current densities in reverse bias, see **Figure 3**a. The *I*–*V* curve departs from a simple ideal diode equation indicating dominant recombination on defect-related states at the junction. Similar diode characteristics were also measured

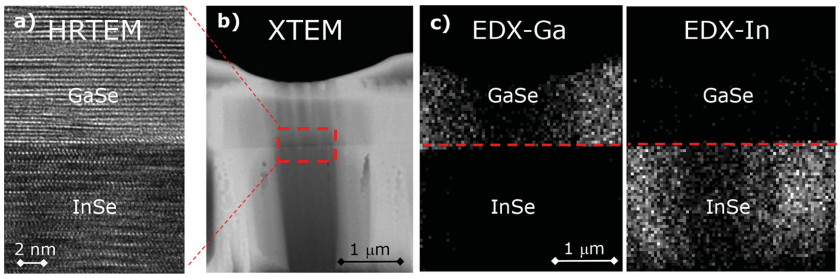

Figure 2. (a) HRTEM, (b) TEM image and (c) EDX maps of a cross-sectional area of a *p*-GaSe/*n*-InSe junction revealing an atomically flat interface between the GaSe and InSe layers. The rectangle in part (b) corresponds to the thinnest cross-sectional part of the sample, from where the HRTEM image in part (a) is acquired. The red lines in the EDX maps in part (c) show the position of the GaSe/InSe interface as determined from the composition of Ga- and In-atoms along the junction. The Fourier Transform analysis of the HRTEM images indicate that the layers are generally misaligned in the plane perpendicular to the *c*-axis.

Adv. Optical Mater. **2014**,
DOI: 10.1002/adom.201400202

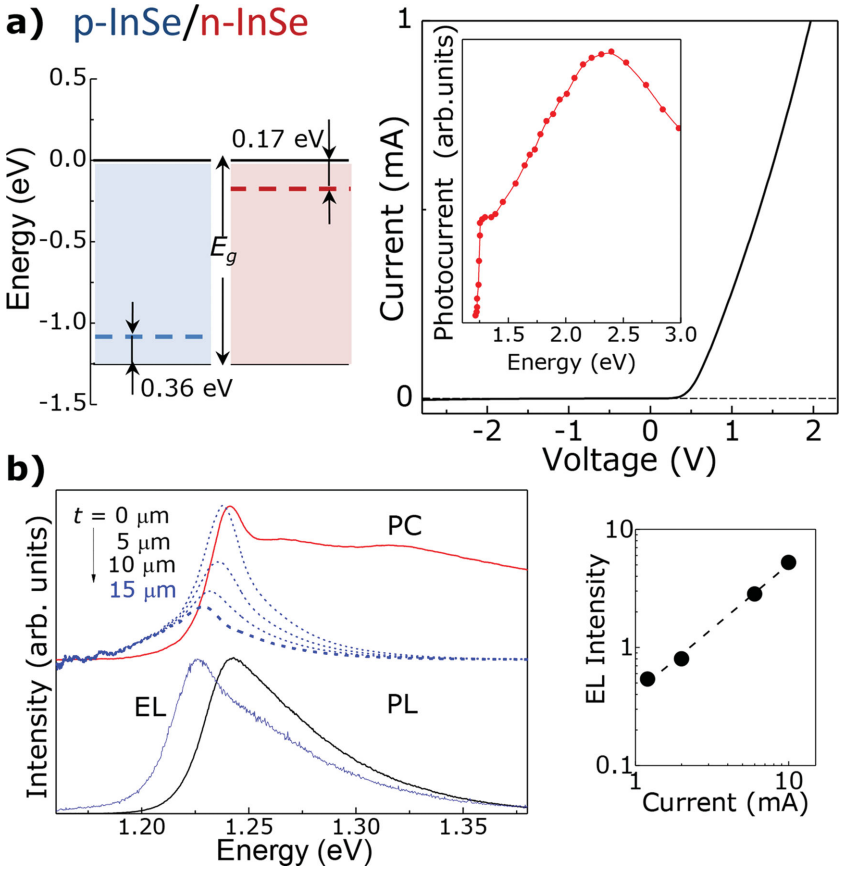

Figure 3. (a) (Left) Band diagrams for isolated *p*- and *n*-type InSe layers. Continuous lines indicate the band edges of the conduction and valence bands; dashed lines correspond to the Fermi levels estimated from the measured carrier density. (Right) Current–voltage characteristics at $T = 300$K and (inset) photoconductivity (PC) spectrum at $V = 0$ V. (b) Normalized EL (blue line, x4; $I = 10$ mA) and PL (black line; $P = 0.1$ mW) spectra at $T = 300$ K. The EL emission is compared with the emission spectra (dashed lines) derived from the measured PC spectrum (red line) by taking into account the absorption of photons through an InSe layer of thickness *t*. The inset on the right shows the dependence of the integrated EL intensity on the current.

in the heterojunctions, see **Figure 4**a. The *I*–*V* curves tend to vary from sample to sample but all show strong rectification at room temperature (*RT*). The *I*–*V* curves were measured over an extended temperature range down to $T = 14$ K: in both the forward-bias and reverse-bias conditions, the magnitude of the current decreases with decreasing *T* due to the influence of the temperature on the diffusion and recombination-generation currents (see Supporting Information S3).

Plots of the room temperature photocurrent versus photon energy are shown in the insets of Figures 3a and 4a indicating a broad-band spectral sensitivity from the near infrared (NIR) to the visible (VIS) parts of the spectrum. For the photocurrent spectrum of the *n*-InSe/*p*-InSe homojunction, the absorption edge is at a photon energy ($h\nu \sim 1.25$ eV) corresponding to the calculated excitonic absorption transition in bulk InSe, which is $h\nu = E_g\text{-}E_b = 1.249$ eV, where $E_g = 1.264$ eV and $E_b = 0.015$ eV are the direct-band gap energy and exciton binding energy in bulk InSe at $T = 300$ K, respectively.[14,21–23] A high energy cut-off of the photoresponse is at $h\nu \sim 2.2$ eV: since the absorption coefficient of InSe increases with energy ($\alpha > 10^4$ cm^{-1} for $h\nu > 2.2$ eV),[23] the high energy incident photons are mostly absorbed near the surface (<1 μm) where the recombination time is short and photocarriers recombine before being collected at the *p*-*n* junction, which is >1 μm below the *n*-InSe top-layer. The heterojunction exhibits a similar behavior except that in this case the sharp cut-off is at $h\nu \sim 2$ eV due to the interband photon absorption in the top *p*-type GaSe layer, whose band gap energy is $E_g = 2.05$ eV at $T = 300$ K.[23] Since all our junctions are based on flakes with thickness $t \geq 1$ μm, quantum confinement effects are not significant. Layers of thickness $t \leq 20$ nm would be required to observe a measurable increase of the direct band gap with decreasing *t*.[14]

For white light excitation with incident power of 100 mW/cm^2, the *n*-InSe/*p*-InSe diodes produce an open-circuit voltage of $V_{oc} \sim 0.6$ V and a short-circuit current density of $J_{sc} \sim 0.7$ mA/cm^2. A larger photoresponse ($V_{oc} \sim 0.6$ V and $J_{sc} \sim 7.5$ mA/cm^2) is observed in the heterojunction since in this case the larger band-gap upper GaSe layer acts as a transparent window for the transmission of light. For an ideal junction, using the band diagrams of the isolated layers[22] and taking into account the energy position of the Fermi-levels (Figures 3a and 4a), we estimate that $V_{oc} = 0.7$ V (homojunction) and $V_{oc} = 0.8$ V (heterojunction), close to the measured values of V_{oc}. The experimental V_{oc}-values can vary slightly in different junctions, thus indicating a possible contribution of crystal defects and impurities to the band alignment. In summary, these diodes exhibit sensitivity to light in the near infrared and visible range of the electromagnetic spectrum at a level that is comparable or better than that reported in the current literature for photodetectors based on other van der Waals crystals, such as MoS_2 and WS_2, which require exfoliation into single layers to become direct-band gap semiconductors, or gating to behave as *p*- or *n*-type semiconductors.[7–10]

We now examine the EL properties of these junctions. In the homojunction, the EL peak is centerd at $h\nu \sim 1.23$ eV, at lower energy with respect to the photoluminescence (PL) emission, Figure 3b. Also, the EL spectrum reveals a weak inflection point at the energy of the PL peak energy, suggesting that the red-shifted EL spectrum arises from the re-absorption of photons in the *n*-type InSe top-layer. To confirm this attribution, we have used the energy dependence of the absorption coefficient, α ($h\nu$), of InSe as derived from the measured PC spectrum and the value of $\alpha = 10^3$ cm^{-1}at the energy of the free exciton absorption at $T = 300$ K.[23] Hence we have derived: *i*) the emission spectrum, $I_0(h\nu)$, using the relation $I_0(h\nu) = \alpha(h\nu)\exp(-h\nu/k_BT)$; and *ii*) the effect on this spectrum of the re-absorption of photons through an InSe layer of thickness *t*, i.e., $I_t(h\nu) = I_0(h\nu)\exp[-\alpha(h\nu)t]$. As shown in Figure 3b, with increasing

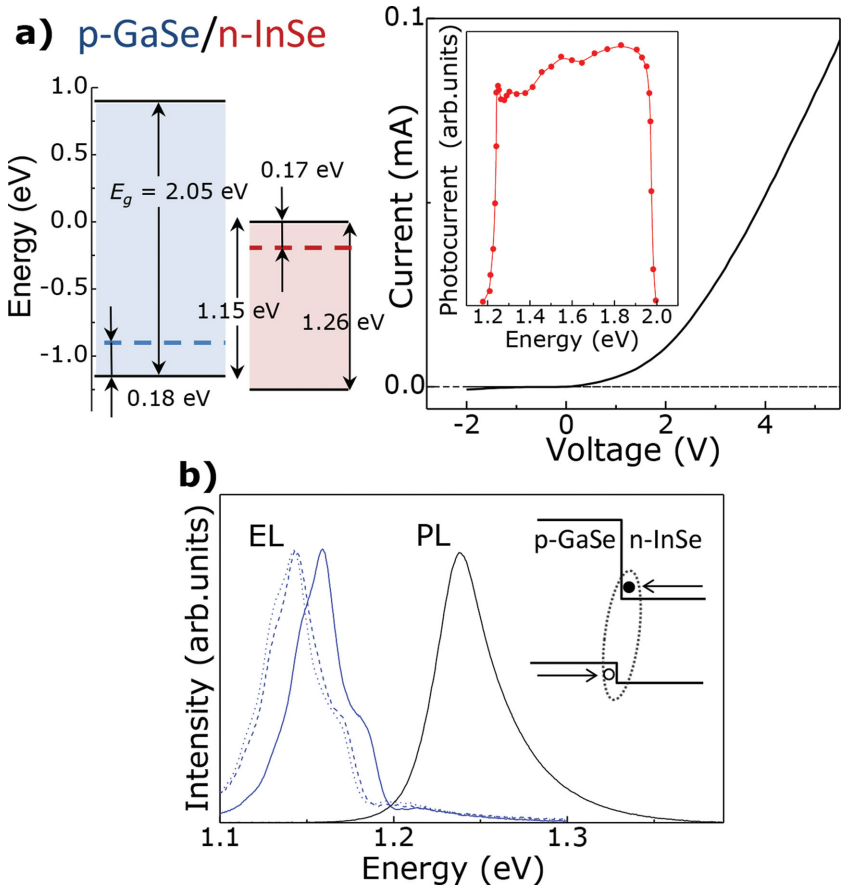

Figure 4. (a) (Left) Band diagrams for isolated *p*-type GaSe and *n*-type InSe layers. Continuous lines indicate the band edges of the conduction and valence bands; dashed lines correspond to the Fermi levels estimated from the measured carrier density. (Right) Current–voltage characteristics at T = 300 K and (inset) photoconductivity spectrum at V = 0 V. (b) Normalized EL spectra (blue lines; I = 0.8 mA (dotted line; x3), 1.8 mA (dashed line; x1.3) and 3.2 mA (continuous line; x1) and PL spectrum (black line, x0.002; P = 0.1 mW) at T = 300 K. The inset sketches the spatially indirect exciton at the GaSe/InSe interface.

t the emission spectrum tends to red-shift relative to the absorption peak; in particular, its energy peak position reproduces the measured EL emission peak energy for t ~ 15 µm. We note that the spectral position of the EL band does not change with increasing current, whereas its intensity scales linearly as expected for a free exciton recombination, rather than for carrier recombination from localized states. Also, with decreasing temperature and at a given applied forward bias, the current decreases, thus leading to a corresponding decrease of the density of injected carriers and of the EL intensity (Supporting Information S3). Thus in the InSe-based homojunctions, holes and electrons are injected from the *p*-type and *n*-type InSe, and exciton generation occurs through direct charge injection at the junction. Since the non-equilibrium carrier concentration in the junction region is much larger than the equilibrium concentration, the dopant-concentration of the *p*- and *n*-layers should not have a significant influence on the EL intensity.

In contrast, the heterojunction diodes exhibit a distinct behavior: the EL emission is peaked at significantly lower energies ($h\nu$ = 1.1–1.2 eV) relative to the PL emission of bulk InSe and its energy position blue-shifts with increasing current, Figure 4b. To understand this behavior we need to consider the band alignment at the heterojunction interface: the conduction minimum (CB) of GaSe lies above that of InSe by ΔE_c = 0.9 eV whereas the valence band (VB) edge of InSe lies below (ΔE_v = –0.1 eV) that of the larger band gap GaSe, resulting in a staggered line up for the holes[22] (inset of Figure 3a). Consequently, the injection of holes and electrons from the *p*-GaSe and *n*-InSe can lead to the formation of spatially indirect excitons with a recombination energy ($h\nu \approx$ 1.15 eV), which is below the energy of the direct exciton recombination in InSe, as we observe.

As the current increases we find: *i*) the intensity of the EL emission tends to saturate; *ii*) the EL band blue-shifts, and *iii*) weak EL features emerge at high photon energy. These observations suggest that carrier recombination involves localized states at the junction interface, which tend to fill with increasing bias. As shown in **Figure 5**, the main EL band can be de-convolved into equally energy spaced Gaussians with energy spacing of ~0.014 eV (116 cm^{-1}), which corresponds to the energy of non-polar optical phonons in InSe.[14–16] In γ-InSe, each unit cell has 12 atoms and 36 vibration modes. The Raman mode at 116 cm^{-1} is the dominant mode observed in the Raman spectra under non-resonant conditions (see ref. [15] and Supporting Information S4). Thus we attribute the EL emission to phonon-assisted electron-hole recombination at the junction interface. Coupling to lattice vibrations can be influenced by local electric fields arising from surface dipoles due to the local atomic structure and charge distribution at the surface of the layers; the degree of coupling to the phonons also increases with the strength of localization particularly for holes due to their larger mass. To estimate the strength of carrier-phonon coupling, we describe the intensity (I) of the main EL emission in Figure 5 by Equation (1):

$$I(h\nu) = \sum_{0}^{\infty} \frac{S^m}{m!} e^{-S} \exp\left[-\frac{(E_0 - h\nu - mh\nu_p)^2}{2\sigma^2}\right], \quad (1)$$

which corresponds to the superposition of a zero-phonon line (m = 0) centered at E_0 and phonon sidebands (m > 0) peaked at E_0-$mh\nu_p$. Here S is the Huang-Rhys factor and $h\nu_p$ = 0.014 eV is the measured phonon energy.[24] In Figure 5, a typical EL spectrum is fitted to Equation (1) with S = 0.6, E_0 = 1.16 eV and m = 3. The high energy part of the EL spectrum is not described by Equation (1), thus suggesting an additional excitonic recombination mechanism involving the absorption of phonons. The specific form of the EL spectrum changes slightly from sample to sample, but the main EL band is always centered at lower energy (~0.1 eV) relative to the band gap energy of InSe, thus indicating a well-defined band lineup at the GaSe/InSe interface.

DOI: 10.1002/adom.201400202

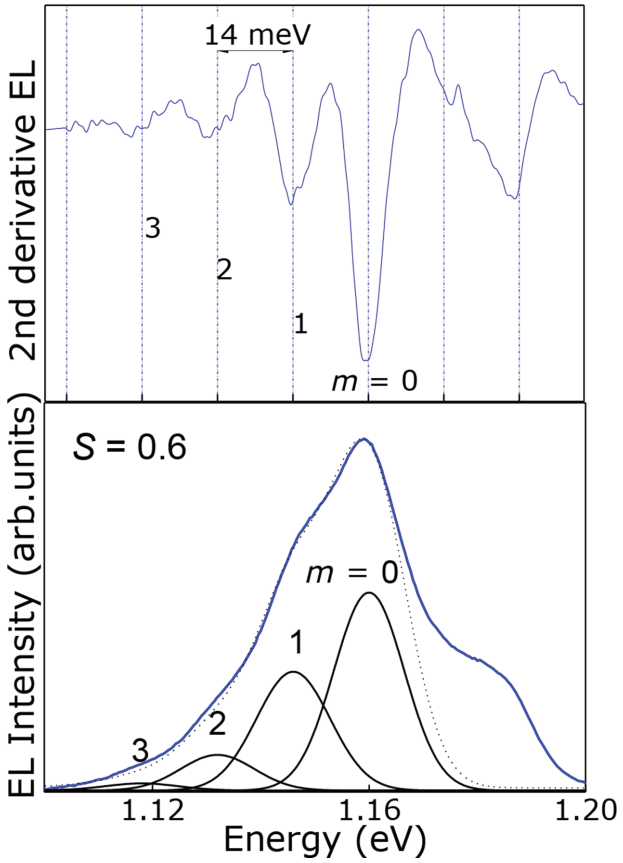

Figure 5. Room temperature EL spectrum and fit by equally spaced Gaussians using Equation (1) in the text. The top figure shows equally spaced minima in the second derivative of the EL spectrum ($I = 3.2$ mA). The energy spacing (0.014 eV) corresponds to the energy of a non-polar phonon of InSe (see also Supporting Information S4).

3. Conclusions

Mechanically formed van der Waals III–VI junctions have atomically flat interfaces, well-defined band lineups and radiative recombination from electrically injected carriers is achieved even in the presence of a large lattice mismatch (~6% for GaSe on InSe) between the constituent layers. Electroluminescence emission can be detected at room temperature in all of the measured *p-n* junctions thus opening realistic prospects for the implementation of these layered crystals in different sequences of layer stacking. These electroluminescent and photon sensitive junctions could be transferred on different substrates (e.g., plastics, graphene, boron nitride, etc.); since these crystals are direct-band semiconductors over a range of thicknesses,[14] down to a few nanometers, they are promising candidates for electronic and optical components in nanoscale optoelectronics and light emitting diodes.

4. Experimental Section

The bulk III–VI crystals were studied by X-ray diffraction (XRD) using a DRON-3 X-ray diffractometer with a monochromatic Cu-Kα radiation of wavelength $\lambda = 1.5418$ Å. The XRD data revealed that the InSe and GaSe crystals had γ- and ε-phase structures, respectively. The experimental set-up for μPL and μEL comprised a He-Ne laser (λ = 633 nm), an XY linear positioning stage, an optical confocal microscope system, a spectrometer with 150 and 1200 groves/mm gratings, equipped with a charge-coupled device and a liquid-nitrogen cooled (InGa)As array photodetector. The laser beam was focused to a diameter $d \sim 1$ μm using 50× and 100× objectives, and the μPL spectra were measured at low power ($P \leq 0.1$ mW) to avoid lattice heating. For the photoconductivity studies, light from a quartz halogen lamp, dispersed through a MDR-23 diffraction grating monochromator, and modulated with a mechanical chopper, was focused onto the junction. The photocurrent signal was measured using a standard lock-in amplification technique.

For the transmission electron microscopy (TEM), high-resolution TEM and energy-dispersive X-ray (EDX) studies, a cross-sectional sample of the junctions was prepared by Ga ion beam thinning and lift-out in an FEI Quanta 3D FIB-SEM equipped with an Omniprobe micromanipulator system. Prior to lift-out, the sample was reinforced with vertical W-support straps to prevent delamination. A section between these straps was subsequently thinned to electron transparency for TEM analysis in a JEOL 2100F FEG-TEM equipped with an Oxford Instruments INCA EDX system.

Acknowledgment

This work is supported by the Engineering and Physical Sciences Research Council (United Kingdom) and The University of Nottingham.

Received: April 30, 2014
Revised: June 23, 2014
Published online:

[1] A. D. Yoffe, *Annu. Rev. Mater. Sci.* **1973**, *3*, 147.
[2] K. S. Novoselov, D. Jiang, F. Schedin, T. J. Booth, V. V. Khotkevich, S. V. Morozov, A. K. Geim, *Proc. Natl. Acad. Sci. USA* **2005**, *102*, 10451.
[3] A. K. Geim, I. V. Grigorieva, *Nature* **2013**, *499*, 419.
[4] T. Georgiou, R. Jalil, B. D. Belle, L. Britnell, R. V. Gorbachev, S. V. Morozov, Y.-J. Kim, A. Gholinia, S. J. Haigh, O. Makarovsky, L. Eaves, L. A. Ponomarenko, A. K. Geim, K. S. Novoselov, A. Mishchenko, *Nature Nanotechnol.* **2013**, *8*, 100.
[5] L. Britnell, R. V. Gorbachev, R. Jalil, B. D. Belle, F. Schedin, A. Mishchenko, T. Georgiou, M. I. Katsnelson, L. Eaves, S. V. Morozov, N. M. R. Peres, J. Leist, A. K. Geim, K. S. Novoselov, L. A. Ponomarenko, *Science* **2012**, *335*, 947.
[6] C. R. Dean, A. F. Young, I. Meric, C. Lee, L. Wang, S. Sorgenfrei, K. Watanabe, T. Taniguchi, P. Kim, K. L. Shepard, J. Hone, *Nature Nanotechnol.* **2010**, *10*, 722.
[7] D. Jariwala, V. K. Sangwan, L. J. Lauhon, T. J. Marks, M. C. Hersam, *ACS Nano* **2014**, *8*, 1102.
[8] W. Jong Yu, Y. Liu, H. Zhou, A. Yin, Z. Li, Y. Huang, X. Duan, *Nature Nanotechnol.* **2013**, *8*, 952.
[9] A. Pospischil, M. M. Furchi, T. Mueller, *Nature Nanotechnol.* **2014**, DOI: 10.1038/nnano.2014.14.
[10] J. S. Ross, P. Klement, A. M. Jones, N. J. Ghimire, J. Yan, D. G. Mandrus, T. Taniguchi, K. Watanabe, K. Kitamura, W. Yao, D. H. Cobden, X. Xu, *Nature Nanotechnol.* **2014**, DOI: 10.1038/nnano.2014.26.
[11] *Electron Spec. Appl. to Low-Dimensional Materials* (Eds: H. P. Hughes, H. I. Starnberg), Kluwer Academic Publishers, Dordrecht, Netherlands **2000**, p 317.
[12] P. Hu, Z. Wen, L. Wang, P. Tan, K. Xiao, *ACS Nano* **2012**, *6*, 5988.
[13] S. Lei, L. Ge, Z. Liu, S. Najmaei, G. Shi, G. You, J. Lou, R. Vajtai, P. M. Ajayan, *Nano Lett.* **2013**, *13*, 2777.

[14] G. W. Mudd, S. A. Svatek, T. H. Ren, A. Patanè, O. Makarovsky, L. Eaves, P. H. Beton, Z. D. Kovalyuk, G. V. Lashkarev, Z. R. Kudrynskyi, A. I. Dmitriev, *Adv. Mater.* **2013**, *25*, 5714.
[15] S. Lei, L. Ge, S. Najmaei, A. George, R. Kappera, J. Lou, M. Chhowalla, H. Yamaguchi, G. Gupta, R. Vajtai, A. D. Mohite, P. M. Ajayan, *ACS Nano* **2014**, *8*, 1263.
[16] a) V. Zólyomi, N. D. Drummond, V. I. Fal'ko, *Phys. Rev. B* **2013**, *87*, 195403; b) V. Zólyomi, N. D. Drummond, V. I. Fal'ko, *Phys. Rev. B* **2014**, *89*, 205416.
[17] K. F. Mak, C. Lee, J. Hone, J. Shan, T. F. Heinz, *Phys. Rev. Lett.* **2010**, *105*, 136805.
[18] A. Splendiani, L. Sun, Y. Zhang, T. Li, J. Kim, C.-Y Chim, G. Galli, F. Wang, *Nano Lett.* **2010**, *10*, 1271.
[19] V. N. Katerinchuk, Z. D. Kovalyuk, V. V. Netyaga, T. V. Betsa, *Inorg. Mater.* **2001**, *37*, 336.
[20] V. N. Katerinchuk, M. Z. Kovalyuk, *Phys. Stat. Sol.* **1992**, *133*, K45.
[21] *Semiconductor: Data Handbook* (Ed: O. Madelung), Springer, London, U.K **2003**, Chap. 23., p. 586.
[22] O. Lang, A. Klein, C. Pettenkofer, W. Jaegermann, A. Chevy, *J. Appl. Phys.* **1996**, *80*, 3817.
[23] A. Segura, J. Bouvier, M. V. Andrés, F. J. Manjón, V. Munõz, *Phys. Rev. B* **1997**, *56*, 4075.
[24] G. B. Bachelet in *Crystalline Semiconducting Materials and Devices* (Eds: P. N. Butcher, N. H. March, M. P. Tosi), Plenum, New York **1986**, p. 243.